

Higgs boson pair production in the little Higgs model at hadron collider ^{*}

Liu Jing-Jing^b, Ma Wen-Gan^{a,b}, Li Gang^b, Zhang Ren-You^b and Hou Hong-Sheng^b

^a CCAST (World Laboratory), P.O.Box 8730, Beijing 100080, P.R.China

^b Department of Modern Physics, University of Science and Technology
of China (USTC), Hefei, Anhui 230027, P.R.China

Abstract

Higgs boson pair production process at hadron collider provides an opportunity for performing the study of the trilinear Higgs boson self-coupling. In this paper, We analyze the pair production of neutral Higgs boson via both gluon-gluon and $b - \bar{b}$ fusions in the littlest Higgs (LH) model at the CERN LHC. We find that in some parameter space the relative corrections of the total cross section to the SM prediction may reach the value of 14% when $x(= 4fv'/v^2) = 0.9$ at the LHC. We conclude that if the parameter x is in the range of 0.85 – 0.9, the effect contributed by the LH model could be observed at the LHC.

PACS: 12.60.Cn, 13.85.Fb, 14.80.Bn

^{*}Supported by National Natural Science Foundation of China.

1 Introduction

The standard model(SM)[1] [2] theory has been proved by all existed precise experimental data with its theoretical predictions beyond one-loop level being coincident with the experimental observations. But in the SM the Higgs boson mass suffers from an instability under radiative corrections. This "hierarchy problem" motivates much of current research works about the new physics beyond the SM. Among the extended models beyond the SM, the little Higgs model offers a very promising solution to the "hierarchy problem" in which the Higgs boson is naturally light as a result of non-linearly realized symmetry[3]-[8]. The first successful model, which cancels all relevant quadratic divergences based on the pseudo-Goldstone idea, was constructed by Arkani-Hamed, Cohen and Georgi[3]. Then more models were constructed, such as $SU(5)/SO(5)$ [6], $SU(6)/SP(6)$ [7], and the minimal moose $SU(3)^2/SU(3)$ [5], general moose $SU(3)^n/SU(3)^k$ [9]. The most economical model of them is the littlest Higgs (LH) model, which is based on an $SU(5)/SO(5)$ nonlinear sigma model[6]. It consists of a $SU(5)$ global symmetry, which is spontaneously broken down to $SO(5)$ by a vacuum condensate f . In the LH model, a set of new heavy gauge bosons (A_H, Z_H, W_H) and a new heavy vector-like quark (T) are introduced which just cancel the quadratic divergence induced by SM gauge boson loops and the top quark loop, respectively.

One of the most important task of the present and future experiments is to search for Higgs boson and investigate its properties. Studying the properties of the Higgs potential will reveal the details of mass-generation mechanism in spontaneously broken gauge theories, which can be obtained through measuring the Higgs boson self-interactions. Multiple

Higgs boson production processes at hadron colliders provide the way to probe the Higgs bosons self-interactions. Many works have been contributed to the studies of the Higgs-pair production at hadron collider in some traditional models[10]-[13]. The possibility of measuring the Higgs boson self-coupling at the LHC has been investigated by U. Baur, T. Plehn and D. Rainwater [14]. They found that it should be possible at the LHC with design luminosity to establish that the SM Higgs boson has non-zero self coupling and that λ/λ_{SM} can be restricted to a range of $0 - 3.7$ at 95% confidence level if its mass is between 150 to 200 *GeV*. Recently, the LH model contribution to Higgs decay width was investigated in Refs. [15] and [19]. C. Dib et al., discussed also the LH model contribution to process $pp \rightarrow H^0H^0 + X$ in Ref.[15]. There they did not consider the mixing and interference effects between the SM particles and the new heavy states, and thus they got the negligible results of the order $(v/f)^4$ and concluded that the contribution from the LH model to the pair production to the Higgs bosons seems to be unobservable at the LHC [15]. If the interference and mixing effects are included in the analysis, the contribution is at the order $(v/f)^2$ and does change obviously the results as compared to the SM prediction in some parameter space[19].

In this paper we investigate the effect of the LH model on neutral Higgs boson pair production via both gluon and bottom fusions at the CERN Large Hadron Collider (LHC) (i.e., $gg \rightarrow H^0H^0$ and $b\bar{b} \rightarrow H^0H^0$) at the complete lowest order, considering the mixing and interference effects between the SM particles and the new heavy states. The paper is organized as follows. In section 2, we briefly go through the LH model theory. In section 3, we present the analytical evaluation. The numerical results, discussions and a short

summary are given in section 4. Finally we present the relevant Feynman rules in the Appendix.

2 The littlest Higgs model

The littlest Higgs (LH) model is based on an $SU(5)/SO(5)$ non-linear sigma model. At the scale $\Lambda_s \sim 4\pi f$, the vacuum expectation value(VEV) associated with the spontaneous symmetry breaking proportional to the scale f is parameterized by the 5×5 symmetry matrix[6][18]

$$\Sigma_0 = \begin{pmatrix} & & \mathbf{1}_{2 \times 2} \\ & 1 & \\ \mathbf{1}_{2 \times 2} & & \end{pmatrix}. \quad (1)$$

The VEV breaks the $SU(5)$ global symmetry into its subgroup $SO(5)$ and breaks the local gauge symmetry $[SU(2) \otimes U(1)]^2$ into its diagonal subgroup $SU(2)_L \otimes U(1)_Y$ at the same time, which is identified as the SM electroweak gauge group. The scalar fields are parameterized by

$$\Sigma(x) = e^{i\Pi(x)/f} \Sigma_0 e^{i\Pi(x)^T/f}, \quad (2)$$

where $\Pi(x) = \pi^a(x)X^a$ is the Goldstone boson matrix. X^a are the broken generators of $SU(5)$ which obey the relation

$$X^a \Sigma_0 - \Sigma_0 X^{aT} = 0. \quad (3)$$

Therefore, the Goldstone boson matrix $\Pi(x)$ can be expressed as

$$\Pi = \begin{pmatrix} & h^\dagger/\sqrt{2} & \phi^\dagger \\ h/\sqrt{2} & & h^*/\sqrt{2} \\ \phi & h^T/\sqrt{2} & \end{pmatrix}, \quad (4)$$

where

$$h = \begin{pmatrix} h^+ & h^0 \end{pmatrix}, \quad \phi = \begin{pmatrix} \phi^{++} & \phi^+/\sqrt{2} \\ \phi^+/\sqrt{2} & \phi^0 \end{pmatrix} \quad (5)$$

are doublet and triplet under the unbroken $SU(2)_L \otimes U(1)_Y$ SM gauge group, respectively.

The leading order dimension-two term for the scalar fields $\Sigma(x)$ in the littlest Higgs model can be written as

$$\mathcal{L} = \frac{1}{2} \frac{f^2}{4} \text{Tr} |\mathcal{D}_\mu \Sigma|^2. \quad (6)$$

\mathcal{D}_μ is the covariant derivative for gauge group $[SU(2) \otimes U(1)]^2 = [SU(2)_1 \otimes U(1)_1] \otimes [SU(2)_2 \otimes U(1)_2]$. It is defined as

$$\mathcal{D}_\mu \Sigma = \partial_\mu \Sigma - i \sum_{j=1}^2 [g_j (W_j \Sigma + \Sigma W_j^T) + g'_j (B_j \Sigma + \Sigma B_j^T)], \quad (7)$$

where $W_{\mu j} = \sum_{a=1}^3 W_{\mu j}^a Q_j^a$ and $B_j = B_{\mu j} Y_j$ are the $SU(2)_j$ and $U(1)_j$ gauge fields, respectively. The generators of two $SU(2)$'s (Q_j^a) and two $U(1)$'s generators (Y_j) are as follows

$$Q_1^a = \begin{pmatrix} \frac{\sigma^a}{2} & \mathbf{0}_{3 \times 3} \end{pmatrix}, \quad Q_2^a = \begin{pmatrix} \mathbf{0}_{3 \times 3} & -\frac{\sigma^{a*}}{2} \end{pmatrix},$$

$$Y_1 = \text{diag}\{-3, -3, 2, 2, 2\}/10, \quad Y_2 = \text{diag}\{-2, -2, -2, 3, 3\}/10, \quad (8)$$

where σ^a ($a = 1, 2, 3$) are the Pauli matrices. As we expect, the breaking of the gauge symmetry $[SU(2) \times U(1)]^2$ into its diagonal subgroup $SU(2)_L \times U(1)_Y$ gives rise to heavy gauge bosons W' and B' , and the remained unbroken subgroup $SU(2)_L \times U(1)_Y$ introduces the massless gauge bosons W and B .

As we know, in the littlest Higgs model there is no Higgs potential at tree-level. Instead, the Higgs potential is generated at one-loop and higher orders due to the interactions

with gauge bosons and fermions. Up to operators of dimension four, the Higgs potential (Coleman-Weinberg potential) can be expressed as [18][19]

$$\begin{aligned} V = & \lambda_{\phi^2} f^2 \text{Tr}(\phi^\dagger \phi) + i \lambda_{h\phi h} f (h \phi^\dagger h^T - h^* \phi h^\dagger) - \mu^2 h h^\dagger + \lambda_{h^4} (h h^\dagger)^2 \\ & + \lambda_{h\phi\phi h} h \phi^\dagger \phi h^\dagger + \lambda_{h^2\phi^2} h h^\dagger \text{Tr}(\phi^\dagger \phi) + \lambda_{\phi^2\phi^2} \left(\text{Tr}(\phi^\dagger \phi) \right)^2 + \lambda_{\phi^4} \text{Tr}(\phi^\dagger \phi \phi^\dagger \phi), \end{aligned} \quad (9)$$

where λ_{ϕ^2} , $\lambda_{h\phi h}$, λ_{h^4} , $\lambda_{h\phi\phi h}$, $\lambda_{h^2\phi^2}$, $\lambda_{\phi^2\phi^2}$ and λ_{ϕ^4} are the coefficients of the original Higgs potential. The coefficients which are concerned in our calculation, have the expressions as[19]

$$\lambda_{\phi^2} = \frac{M_\phi^2}{f^2}, \quad \lambda_{h\phi h} = \frac{x M_\phi^2}{2f^2}, \quad \lambda_{h^4} = \frac{M_\phi^2}{4f^2}, \quad \lambda_{h\phi\phi h} = -\frac{4M_\phi^2}{3f^2}. \quad (10)$$

By minimizing the Coleman-Weinberg potential, we obtain the vacuum expectation values $\langle h^0 \rangle = v/\sqrt{2}$, $\langle i\phi^0 \rangle = v'$ of the Higgs boson doublet h and triplet ϕ , which give rise to the electroweak symmetry breaking (EWSB). The Coleman-Weinberg potential provides the trilinear and quartic Higgs self-couplings. After EWSB, the gauge sector gets additional mass and mixing term due to the VEVs of h and ϕ . By diagonalizing the quadratic term of the gauge sector, we may get the mass eigenstates A_L , Z_L , W_L , A_H , Z_H and W_H , and their masses.

To avoid large quadratic divergence in the Higgs boson mass due to the heavy top Yukawa interaction, we introduce a pair of new fermions \tilde{t} and \tilde{t}' [6][18] and a set of new interactions. The scalar couplings to the top quark can be taken from the following Lagrangian [6][18]:

$$\mathcal{L}_Y = \frac{1}{2} \lambda_1 f \epsilon_{ijk} \epsilon_{xy} \chi_i \Sigma_{jx} \Sigma_{ky} u_3'^c + \lambda_2 f \tilde{t} \tilde{t}'^c + h.c. \quad (11)$$

where $\chi = (b_3, t_3, \tilde{t})$, ϵ_{ijk} and ϵ_{xy} are antisymmetric tensors where i, j, k run through 1, 2, 3 and x, y run through 4, 5, and λ_1 and λ_2 are the new model parameters. By expanding the above Lagrangian, we get the physical states of the top quark t and a new heavy vector-like quark T . The masses of the two physical states are

$$m_t = \frac{v\lambda_1\lambda_2}{\sqrt{\lambda_1^2 + \lambda_2^2}} \left\{ 1 + \frac{v^2}{f^2} \left[-\frac{1}{3} + \frac{fv'}{v^2} + \frac{1}{2} \frac{\lambda_1^2}{\lambda_1^2 + \lambda_2^2} \left(1 - \frac{\lambda_1^2}{\lambda_1^2 + \lambda_2^2} \right) \right] \right\}, \quad (12)$$

$$m_T = f \sqrt{\lambda_1^2 + \lambda_2^2} [1 + \mathcal{O}(v^2/f^2)], \quad (13)$$

respectively. Since the top quark mass is already obtained in the SM, we can then get the parameter relation from Eq.(12) as deduced in Ref.[18]

$$\frac{1}{\lambda_1^2} + \frac{1}{\lambda_2^2} \approx \frac{v^2}{m_t^2} \approx 2. \quad (14)$$

3 Calculation

At hadron collider, the Higgs boson pair can be produced through two mechanisms. One is loop induced production via gluon fusion, the other is from $b\bar{b}$ -annihilation. The Feynman diagrams contributing to the subprocess $gg \rightarrow H^0 H^0$, which are involved in the framework of the LH model, are depicted in Fig.1. The diagrams created by exchanging two external gluon lines and final Higgs boson lines are not shown there. In Fig.1, the first three diagrams(Fig.1(1)-(3)) (excluding the Fig.1(1) with a heavy vector-like quark (T) loop) are just the same as those in the framework of the SM, while the rest four figures (Fig.1((4)-(7)) are the extra diagrams beyond the SM. All the Feynman diagrams can be classified into three types. The first type is named as s-channel diagrams with exchange of a virtual

neutral Higgs boson H^0 or heavy triplet Higgs boson Φ^0 which couples to a pair of gluons via a triangle quark loop(shown in Fig.1(1),(4)). The second type is called box diagrams (shown in Fig.1((2)-(3)),((5)-(6))) and the third is the quartic interaction type where the neutral Higgs bosons are produced by means of quartic interactions (shown in Fig.1(7)). All the relevant Feynman rules can be found in Ref.[18] and the Appendix in this paper. In the loop diagram calculation of this subprocess, we adopt dimensional regularization scheme. The Feynman diagrams for subprocess $b\bar{b} \rightarrow H^0H^0$ are depicted in Fig.2. In this work we adopted the Feynman-'t Hooft gauge.

In our calculation, we denote the two subprocesses as

$$g(c_1, p_1) + g(c_2, p_2) \rightarrow H^0(k_1) + H^0(k_2), \quad (15)$$

$$b(c_3, p_1) + \bar{b}(c_4, p_2) \rightarrow H^0(k_1) + H^0(k_2). \quad (16)$$

where c_1, c_2, c_3 and c_4 are the color indexes of the two initial particles (gg and $b\bar{b}$). p_1, p_2 and k_1, k_2 are the incoming and outgoing four-momenta of initial and final particles, respectively. In the subprocess $gg \rightarrow H^0H^0$, we define θ as the scattering angle between one of the gluons and one of the final H^0 bosons, and in the subprocess $b\bar{b} \rightarrow H^0H^0$, θ represents the scattering angle between the b quark and one of final Higgs bosons. In the center of mass system (CMS) the four-momenta of the initial and final particles can be expressed as ¹

$$p_1 = \left(\frac{\sqrt{\hat{s}}}{2}, 0, 0, \frac{\sqrt{\hat{s}}}{2} \right),$$

¹In our calculation we set the mass of the b quark to be zero except in the Yukawa coupling.

$$\begin{aligned}
p_2 &= \left(\frac{\sqrt{\hat{s}}}{2}, 0, 0, -\frac{\sqrt{\hat{s}}}{2} \right), \\
k_1 &= \left(\frac{\sqrt{\hat{s}}}{2}, \frac{\sqrt{\hat{s}}}{2} \beta_{H^0} \sin \theta, 0, \frac{\sqrt{\hat{s}}}{2} \beta_{H^0} \cos \theta \right), \\
k_2 &= \left(\frac{\sqrt{\hat{s}}}{2}, -\frac{\sqrt{\hat{s}}}{2} \beta_{H^0} \sin \theta, 0, -\frac{\sqrt{\hat{s}}}{2} \beta_{H^0} \cos \theta \right),
\end{aligned} \tag{17}$$

where $\beta_{H^0} = \sqrt{1 - 4m_{H^0}^2/\hat{s}}$ is the velocity of final neutral Higgs bosons in the CMS and $\hat{s} = (p_1 + p_2)^2$.

The amplitude for the subprocess $gg \rightarrow H^0 H^0$ can be expressed as

$$\begin{aligned}
\mathcal{M}(gg \rightarrow H^0 H^0) &= \mathcal{M}^{(t)} + \mathcal{M}^{(b)} + \mathcal{M}^{(q)} \\
&= \epsilon_\mu(p_1) \epsilon_\nu(p_2) \left(f_1 g^{\mu\nu} \delta_{c_1 c_2} + f_2 k_1^\mu k_1^\nu \delta_{c_1 c_2} + f_3 \epsilon^{\alpha\mu\nu\beta} k_{1\alpha} p_{1\beta} \right. \\
&\quad \left. + f_4 \epsilon^{\alpha\mu\nu\beta} k_{1\alpha} p_{2\beta} + f_5 \epsilon^{\mu\nu\alpha\beta} p_{1\alpha} p_{2\beta} \right)
\end{aligned} \tag{18}$$

where $\mathcal{M}^{(t)}$, $\mathcal{M}^{(b)}$ and $\mathcal{M}^{(q)}$ represent the amplitudes of triangle, box and quartic diagrams, respectively.

For the subprocess $b\bar{b} \rightarrow H^0 H^0$, the amplitude can be expressed as

$$\mathcal{M}(b\bar{b} \rightarrow H^0 H^0) = \bar{v}(p_2) (g_1 + g_2 \not{k}_1) \delta_{c_3 c_4} u(p_1). \tag{19}$$

In above two equations f_i ($i = 1, \dots, 5$) and g_j ($j = 1, 2$) are the form factors of the two subprocesses, respectively. Since the explicit expressions of these form factors are lengthy, we do not list them in this paper.²

Then the total cross sections for these two subprocesses can be written in the forms as

$$\hat{\sigma}(\hat{s}, gg \rightarrow H^0 H^0) = \frac{1}{32\pi\hat{s}^2} \int_{\hat{t}^-}^{\hat{t}^+} d\hat{t} \overline{\sum} |\mathcal{M}(gg \rightarrow H^0 H^0)|^2, \tag{20}$$

$$\hat{\sigma}(\hat{s}, b\bar{b} \rightarrow H^0 H^0) = \frac{1}{32\pi\hat{s}^2} \int_{\hat{t}^-}^{\hat{t}^+} d\hat{t} \overline{\sum} |\mathcal{M}(b\bar{b} \rightarrow H^0 H^0)|^2, \tag{21}$$

²The Mathematica program codes of all the form factors for $gg \rightarrow H^0 H^0$ and $b\bar{b} \rightarrow H^0 H^0$ are obtainable by sending email to moonbank@mail.ustc.edu.cn .

respectively, where the bar over summation recalls averaging over initial spins and colors, $\hat{t}^\pm = (m_{H^0}^2 - \hat{s}/2 \pm \hat{s}\beta_{H^0}/2)$ and due to the identical final two Higgs bosons, the right-hand sides of Eqs.(20) and (21) have been multiplied by an additional factor 1/2 separately. The color and spin average factors for the subprocess $gg \rightarrow H^0H^0$ are 1/64 and 1/4, and for the subprocess $b\bar{b} \rightarrow H^0H^0$ are 1/9 and 1/4, respectively. The total cross section for the neutral Higgs boson pair production through gluon (or bottom) fusion in proton-proton collisions can be obtained by doing the following integration

$$\sigma(pp \rightarrow gg(b\bar{b}) \rightarrow H^0H^0) = \int_{4m_{H^0}^2/s}^1 d\tau \frac{dL_{ij}}{d\tau} \hat{\sigma}(\hat{s} = \tau s, gg(b\bar{b}) \rightarrow H^0H^0), \quad (22)$$

where \sqrt{s} and $\sqrt{\hat{s}}$ denote the pp and gg (or $b\bar{b}$) CMS energies respectively, and $dL_{ij}/d\tau$ is the luminosity of colliding partons, which is defined as

$$\frac{dL_{ij}}{d\tau} = \frac{1}{1 + \delta_{ij}} \int_\tau^1 \frac{dx_1}{x_1} \left[F_{i/p}(x_1, \mu) F_{j/p}(\frac{\tau}{x_1}, \mu) + (i \leftrightarrow j) \right]. \quad (23)$$

In our calculation we adopt the CTEQ6 parton distribution function [21] and take the factorization scale μ to be $2m_{H^0}$ in the subprocess $gg \rightarrow H^0H^0$, while μ to be $m_{H^0}/2$ in the calculation of the subprocess $b\bar{b} \rightarrow H^0H^0$ [22]. The numerical calculation is carried out for the LHC at the energy of 14 TeV.

4 Numerical results and discussions

In the numerical evolution we take the input parameters as: $m_W = 80.423$ GeV, $m_Z = 91.1876$ GeV, $m_u = 4.5$ MeV, $m_d = 8.5$ MeV, $m_s = 150$ MeV, $m_c = 1.25$ GeV, $m_t = 174.3$ GeV, and $\alpha(m_Z) = 1/128$. We use a simple one-loop formula to express the running

strong coupling constant α_s

$$\alpha_s(\mu) = \frac{\alpha_s(m_Z)}{1 + \frac{33-2n_f}{6\pi} \alpha_s(m_Z) \ln(\frac{\mu}{m_Z})}. \quad (24)$$

where $\alpha_s(m_Z) = 0.118$ and n_f is the number of active flavors at scale μ [16].

In the numerical calculation, we use the next-to-leading order formula to evaluate the running mass of bottom quark $\overline{m}_b(Q)$ [17].

$$\begin{aligned} \overline{m}_b(Q) &= U_5(Q, \overline{m}_b) \overline{m}_b(\overline{m}_b), & Q < m_t, \\ \overline{m}_b(Q) &= U_6(Q, m_t) U_5(m_t, \overline{m}_b) \overline{m}_b(\overline{m}_b), & Q > m_t. \end{aligned} \quad (25)$$

where $\overline{m}_b = \overline{m}_b(\overline{m}_b) = 4.25 \text{ GeV}$ and the energy scale Q is taken to be $2m_{H^0}$ in our calculation. The evolution factor $U_f(f = 5, 6)$ is

$$\begin{aligned} U_f(Q_2, Q_1) &= \left(\frac{\alpha_s(Q_2)}{\alpha_s(Q_1)} \right)^{d^f} \left[1 + \frac{\alpha_s(Q_1) - \alpha_s(Q_2)}{4\pi} J^f \right], \\ d^f &= \frac{12}{32 - 2f}, \\ J^f &= -\frac{8982 - 504f + 40f^2}{3(33 - 2f)^2}. \end{aligned} \quad (26)$$

In the LH model, the calculation of the Higgs boson pair production at hadron colliders involves four additional free parameters. One is the parameter f , which is the symmetry breaking scale parameter at TeV order. The direct and indirect effects of the LH model provided by present experimental measurements have placed constraint $f \gtrsim 3.5 \text{ TeV}$, although it depends on the model assumption about the $U(1)'s$ [18][20][23]. The second one is the mass of the Higgs boson m_{H^0} . The third parameter is the coefficient λ_2 , which is the coupling constant of the new heavy vector-like quark T . Because there is a relation between the top quark and heavy vector-like quark coupling parameters λ_1 and λ_2 , as

shown in Eq.(14), we can use λ_1/λ_2 to parameterize the mass of new heavy vector quark (see Eq.(13)). The last one is v' , and we define $x = 4fv'/v^2$ to parameterize this vacuum expectation value of the scalar triplet field ϕ . The masses of neutral scalar boson M_{Φ^0} can be given as[18][19]

$$M_{\Phi^0}^2 = \frac{2m_{H^0}^2 f^2}{v^2(1 - (4v'f/v^2)^2)} = \frac{2m_{H^0}^2 f^2}{v^2(1 - x^2)}. \quad (27)$$

The above equation about the mass of Φ requires the constraint of $0 \leq x < 1$ (i.e. $4v'f/v^2 \lesssim 1$), which shows the relation between the scale f and the vacuum expectation values of Higgs field doublet and triplet(v, v'). Based on the limitation of current electroweak experimental data [18][20][23], in our calculation we choose $f = 3.5$ TeV unless otherwise stated.

Since our numerical calculation shows that the contributions of subprocess $b\bar{b} \rightarrow H^0 H^0$ to the parent process $pp \rightarrow H^0 H^0 + X$ at the LHC is less than 1% of the contributions from subprocess $gg \rightarrow H^0 H^0$, we present only the plots about the subprocess $gg \rightarrow H^0 H^0$ for representation. In fact, our analysis also demonstrates that the contributions of the additional diagrams involving the new heavy vector-like quark T or neutral heavy triplet Higgs boson Φ^0 for the subprocess $gg \rightarrow H^0 H^0$, are very small. The deviations of the cross section from the SM are mainly aroused by the contributions of the diagrams which exist also in the SM, but the interactions between Higgs boson and quarks in the LH model are different with corresponding ones in the SM.

The relative effect of the LH on the cross section ($\delta = (\hat{\sigma}_{LH} - \hat{\sigma}_{SM})/\hat{\sigma}_{SM}$) for subprocess $gg \rightarrow H^0 H^0$ as the functions of the CMS energy ($\sqrt{\hat{s}}$) of incoming gluons for the cases of $x = 0$ (corresponding to $M_{\Phi^0} = 3.06$ TeV) and $x = 1/\sqrt{2}$ (corresponding to $M_{\Phi^0} =$

4.32 TeV) are depicted in Fig.3(a)-(1) and Fig.3(a)-(2) separately, with the parameters taken as $f = 3.5$ TeV and $m_{H^0} = 150$ GeV. In both figures, the full-line, dashed-line and dotted-line correspond to $\lambda_1/\lambda_2 = 1/2$, $\lambda_1/\lambda_2 = 1$ and $\lambda_1/\lambda_2 = 2$, respectively. From Eq.(12-14) we can get that those curves correspond to $m_T = 6.28$ TeV, 5 TeV and 6.28 TeV, separately. All the curves in Fig.3(a)-(1)(2) have the common line structure which decreases rapidly in the vicinity of the Higgs boson pair production threshold with the increment of $\sqrt{\hat{s}}$, and then increases steadily after arriving its minimal value. The curves also obviously show that with the increase of the value of λ_1/λ_2 , the effect of the LH model is getting more stronger.

In order to clarify the line shape in Fig.3(a) more clearly, we present the cross sections in the LH model($\hat{\sigma}_{LH}$), the SM($\hat{\sigma}_{SM}$) and the difference between them ($\hat{\sigma}_{LH} - \hat{\sigma}_{SM}$) for the subprocess $gg \rightarrow H^0H^0$ as the functions of $\sqrt{\hat{s}}$ with $m_{H^0} = 150$ GeV, $f = 3.5$ TeV, $\lambda_1/\lambda_2 = 1$ and $x = 0$ in Fig.3(b) and Table 1. The full-line, dashed-line and dotted-line in Fig.3(b) correspond to $\hat{\sigma}_{SM}$, $\hat{\sigma}_{LH}$ and $\hat{\sigma}_{LH} - \hat{\sigma}_{SM}$, respectively. We can see from Fig.3(b) that in the $\sqrt{\hat{s}}$ region from 310 GeV to 500 GeV the curve for $\hat{\sigma}_{SM}$ raises up steeply, while the $\hat{\sigma}_{LH} - \hat{\sigma}_{SM}$ changes gently, which can be also read out from Table 1. Fig.3(b) and Table.1 show that the pole like behavior of the CMS energy around $\sqrt{\hat{s}} \sim 400$ -500 GeV in Fig.3(a)-(1)(2), comes from the fact that the cross section($\hat{\sigma}_{SM}$) raises up steeply when $\sqrt{\hat{s}}$ is just beyond the threshold energy and decrease gently after $\hat{\sigma}_{SM}$ reaches its maximal value (400-500 GeV), while the variation of $\hat{\sigma}_{LH} - \hat{\sigma}_{SM}$ is relatively slow in our plotted energy range.

The dependence of the ratio $\hat{\sigma}_{LH}/\hat{\sigma}_{SM}$ of the subprocess $gg \rightarrow H^0H^0$ on the parameter

$\sqrt{\hat{s}}$	$\hat{\sigma}_{SM}$	$\hat{\sigma}_{LH}$	$\hat{\sigma}_{LH} - \hat{\sigma}_{SM}$	$(\hat{\sigma}_{LH} - \hat{\sigma}_{SM})/\hat{\sigma}_{SM}$
310	0.0052071	0.0060828	0.0008756	0.168162
330	0.0268346	0.0295622	0.0027275	0.101643
350	0.0884609	0.0947308	0.0062699	0.0708781
370	0.2052696	0.2169084	0.0116388	0.0567002
400	0.3425389	0.3595995	0.0170606	0.0498064
420	0.4051675	0.4245253	0.0193578	0.0477772
440	0.4476802	0.4685783	0.0208981	0.0466808
460	0.4738619	0.4957345	0.0218726	0.0461582
490	0.4903020	0.5128817	0.0225796	0.0460525
500	0.4912129	0.5138794	0.0226666	0.0461441
520	0.4880278	0.5107043	0.0226765	0.0464655
540	0.4797802	0.5022973	0.0225171	0.0469321
590	0.4462748	0.4679308	0.0216559	0.048526
700	0.3565471	0.3754663	0.0189191	0.0530621
900	0.2334130	0.2478193	0.0144063	0.06172
1000	0.1935886	0.2063001	0.0127115	0.0656626
2000	0.0598705	0.0659044	0.0060339	0.100783

Table 1: The cross sections of $gg \rightarrow H^0 H^0$ in the LH model and SM, the difference between them and the relative correction with $m_{H^0} = 150$ GeV, $f = 3.5$ TeV, $\lambda_1/\lambda_2 = 1$ and $x = 1/\sqrt{2}$

x with $m_{H^0} = 150$ GeV and $\sqrt{\hat{s}} = 800$ GeV, is depicted in Fig.4(a). The full-line, dashed-line and dotted-line correspond to $\lambda_1/\lambda_2 = 1/2$, $\lambda_1/\lambda_2 = 1$ and $\lambda_1/\lambda_2 = 2$, respectively. Fig.4(a) shows that the effect of the LH model always enhances the cross section of $gg \rightarrow H^0 H^0$ in our chosen parameter space. The three curves also demonstrate that the effect of the LH model is not sensitive to x in the range of $x \lesssim 0.8$, but their values increase rapidly and can be larger than 1.1 when $x > 0.85$ for all three curves. To explain the result that the correction blows up as we take $x \rightarrow 1$ limit shown in Fig.4(a), we decompose the cross sections of subprocess $gg \rightarrow H^0 H^0$ in the LH model into three parts,

$$\hat{\sigma}_{LH} = \hat{\sigma}_{box} + \hat{\sigma}_{tri} + \hat{\sigma}_{int}. \quad (28)$$

where we denote $\hat{\sigma}_{box}$, $\hat{\sigma}_{tri}$ and $\hat{\sigma}_{int}$ as the contribution parts from the box diagrams(including quartic diagrams, shown in Fig.1(2)-(3),(5)-(7)), the triangle diagrams(shown in Fig.1(1),(4)) and the interference between the box and triangle diagrams respectively. In Fig.4(b), we show the contributions of these three parts as the functions of x with the conditions of $\sqrt{s} = 800$ GeV, $m_{H^0} = 150$ GeV, $f = 3.5$ TeV and $\lambda_1/\lambda_2 = 1$. The full-line, dotted-line, dash-dotted line and dashed-line correspond to box diagrams, triangle diagrams, interference contributions and total cross section respectively. Our calculation demonstrates that the main contribution to the cross section of subprocess $gg \rightarrow H^0 H^0$ comes from the box diagrams, and the interference contribution is mainly from the Feynman diagrams involving top quark. Let's review the couplings of $H^0 - H^0 - H^0$ and $H^0 - \bar{t} - t$ in the LH model. They can be expressed as follows,

$$g_{H^0 H^0 H^0} : -i \left(\frac{3m_{H^0}^2}{v} - \frac{33m_{H^0}^2 v}{4f^2} \frac{x^2}{1-x^2} \right) \quad (29)$$

$$g_{H^0 \bar{t} t} : -i \frac{m_t}{v} \left[1 + \frac{xv^2}{2f^2} - \frac{x^2 v^2}{4f^2} - \frac{2}{3} \frac{v^2}{f^2} + \frac{v^2}{f^2} \frac{\lambda_1^2}{\lambda_1^2 + \lambda_2^2} \left(1 + \frac{\lambda_1^2}{\lambda_1^2 + \lambda_2^2} \right) \right]. \quad (30)$$

We can see that the contribution of the triangle Feynman diagrams is s-channel suppressed and is relative small, due to the heavy Φ^0 and $\sqrt{s} = 800$ GeV $\gg m_{H^0}$. The figure shows that the contribution from the interference between the box diagrams and triangle diagrams is negative and blows up quickly when we take $x \rightarrow 1$ limit. We also find the dependence of the product of $g_{H^0 H^0 H^0}$ and $g_{H^0 \bar{t} t}$ on parameter x behaves the same rapid increment when x is close to 1. Therefore, we can conclude that the quick enhancement behavior of the total cross section in the vicinity where $x \rightarrow 1$, arises mainly from the contributions of interference between the triangle diagrams involving $g_{H^0 H^0 H^0}$ vertex

and the box diagrams involving $g_{h^0\bar{t}t}$ coupling. But $x \rightarrow 1$ cannot be a very well defined limit since we started with a relatively well behaved Higgs potential. Perturbativity alone should also put some bounds on the range that x should be allowed to vary. Although we cannot predict the definitive limitations of the Higgs potential parameters, their size should be roughly order one theoretically. We depict the relations between x (or g_{HHH}) and the absolute values of original Higgs potential parameters λ_{ϕ^2} , $\lambda_{h\phi h}$, λ_{h^4} and $\lambda_{h\phi\phi h}$ (see Eq.(10)) in Fig.4(c) in the conditions of $f = 3.5$ TeV and $m_{H^0} = 150$ GeV. In the figure, the full-line, dashed-line, dotted-line and dash-dotted line correspond to $|\lambda_{\phi^2}|$, $|\lambda_{h\phi h}|$, $|\lambda_{h^4}|$ and $|\lambda_{h\phi\phi h}|$, respectively. The absolute value of coupling $g_{H^0H^0H^0}$ corresponding to the x value is scaled on the upper axis. From the figure, we can see that the values of the Higgs potential parameters increase rapidly when $x \gtrsim 0.9$, which are far greater than unite and cannot satisfy the perturbative request. Therefore, we can put the bounds on the varying range of the parameter x , i.e., $0 < x < 0.9$.

The ratio of total cross sections σ_{LH}/σ_{SM} as the functions of x at the LHC ($\sqrt{s} = 14$ TeV) with $f = 3.5$ TeV and $\lambda_1/\lambda_2 = 2$ is depicted in Fig.5. The total cross section involves the contributions of both subprocesses $gg \rightarrow H^0H^0$ and $b\bar{b} \rightarrow H^0H^0$. In the figure, the full-line, dashed-line and dotted-line correspond to $m_{H^0} = 115$ GeV, 150 GeV and 180 GeV respectively. We can see again that the deviation of total cross section in the LH model from the corresponding SM value, is not sensitive to x when $x \lesssim 0.8$, but increases quickly when $x > 0.9$, and the relative deviation, defined as $\delta = (\sigma_{LH} - \sigma_{SM})/\sigma_{SM}$, can be beyond 12% when x reach 0.9 at the LHC. We can see from this figure that the correction effect of the LH model is obviously related to the Higgs boson mass. When the Higgs mass

varies in the range of 115 GeV to 180 GeV, the curves show that the heavier the Higgs boson mass is, the stronger the correction effect becomes.

In Fig.6 we plot the ratio between the total cross sections in the LH model and the SM, as the functions of the mass of neutral Higgs boson m_{H^0} with the conditions of $f = 3.5$ TeV and $\lambda_1/\lambda_2 = 2$ at the LHC. In this figure, the full-line, dashed-line and dotted-line correspond to the cases of $x = 0, 1/\sqrt{2}$ and 0.9 respectively. The relative correction of the LH model to the SM cross section ($\delta = (\sigma_{LH} - \sigma_{SM})/\sigma_{SM}$), can reach 14% when $x = 0.9$ at the LHC.

The total cross sections σ_{SM} and σ_{LH} of process $pp \rightarrow H^0H^0$ as the functions of the mass of neutral Higgs boson m_{H^0} is depicted in Fig.7 at the LHC, with $f = 3.5$ TeV, $x = 0.9$ and $\lambda_1/\lambda_2 = 2$ in the LH model. The full-line and the dashed-line correspond to the cases of the SM and the LH model, respectively. They show that the absolute correction induced by the LH model decreases with the increase of the Higgs boson mass.

In Fig.8, we plot the total cross sections σ_{LH} of process $pp \rightarrow H^0H^0$ as the functions of the new heavy vector-like quark mass m_T with $m_{H^0} = 150$ GeV and $x = 1/\sqrt{2}$ in the LH model at the LHC. In this figure the full-line is for $\lambda_1/\lambda_2 = 1/2$, dashed-line for $\lambda_1/\lambda_2 = 1$ and dotted-line for $\lambda_1/\lambda_2 = 2$. According to Eq.(13) for a fixed value of λ_1/λ_2 , the mass of heavy vector-like quark T is only related to the symmetry breaking scale parameter f . For example, when $\lambda_1/\lambda_2 = 2$ and m_T varies from 1.5 TeV to 4.0 TeV, we have parameter f changes from 0.85 TeV to 2.26 TeV. We can see from this figure that in the chosen parameter space the cross sections are enhanced, when either m_T is relative small or λ_1/λ_2 is relative larger.

In conclusion, we investigated the effect of the LH model on the pair production process of neutral Higgs boson via both gluon and bottom fusions at the LHC. The numerical analysis shows that with the possible parameters, the relative cross section correction to the SM prediction may reach the value of 14% at the LHC when $x = 0.9$. We conclude that when the parameter x is in the range of $0.85 - 0.9$, the effect on the cross section contributed by the LH model to the process $pp \rightarrow H^0 H^0 + X$ could be observable at the LHC.

Acknowledgement: This work was supported in part by the National Natural Science Foundation of China and a grant from the University of Science and Technology of China.

Appendix

The interactive Lagrangian of the scalar field Σ and the up-type quarks of the first two generations take the same form as in Eq.(11), except that there is no need for the extra \tilde{t} . The interactive Lagrangian of the Σ and the down-type quarks can be expressed as

$$\mathcal{L}_Y = \frac{1}{2} \lambda_d f \epsilon_{ijk} \epsilon_{xy} \chi_i \Sigma_{jx}^* \Sigma_{ky}^* d^c + h.c. \quad (31)$$

where the isospin index $i = 1, 2$. All the Yukawa couplings between Higgs boson and quarks (except the Yukawa coupling which involves the top quark) can be obtained from the corresponding Lagrangian directly. We present the expressions of the $H^0 - H^0 - \bar{u} - u$ and $H^0 - H^0 - \bar{d} - d$ couplings in the following equations.

$$g_{H^0 H^0 \bar{d}d} : -i \frac{4m_d v'}{v^2(f + v')} , \quad g_{H^0 H^0 \bar{u}u} : -i \frac{4m_u v'}{v^2(f + v')} . \quad (32)$$

The expressions of other concerning couplings in this work can be found in Ref.[18].

In the LH model, the trilinear interaction of Higgs bosons $g_{H^0H^0H^0}$ gets correction to the SM at order of v^2/f^2 , and additional $H^0H^0\Phi^0$ coupling is generated. They are given by the following Lagrangians:

$$\begin{aligned}-\mathcal{L}_{HHH} &= H^0H^0H^0 \left(-\frac{2fv'\lambda_{h\phi h}}{v} + v\lambda_{h^4} - \frac{12v'^2\lambda_{h^4}}{v} + \frac{6v'^2\lambda_{h\phi\phi h}}{v} \right), \\ -\mathcal{L}_{HH\phi} &= H^0H^0\phi^0 \left(-\frac{f\lambda_{h\phi h}}{\sqrt{2}} + \frac{14\sqrt{2}fv'^2\lambda_{h\phi h}}{v^2} - 6\sqrt{2}v'\lambda_{h^4} + \frac{5v'\lambda_{h\phi\phi h}}{\sqrt{2}} \right).\end{aligned}\quad (33)$$

From above Lagrangians we obtain the Feynman rule for $H^0H^0H^0$ and $H^0H^0\Phi^0$ couplings as [18] :

$$\begin{aligned}g_{H^0H^0H^0} &: -i \left(\frac{3m_{H^0}^2}{v} - \frac{66M_{\Phi^0}^2v'^2}{f^2v} \right), \\ g_{H^0H^0\phi^0} &: -i \left(\frac{56\sqrt{2}M_{\Phi^0}^2v'^3}{v^4} - \frac{2\sqrt{2}M_{\Phi^0}^2v'}{v^2} - \frac{29\sqrt{2}M_{\Phi^0}^2v'}{3f^2} \right).\end{aligned}\quad (34)$$

References

- [1] S. L. Glashow, Nucl. Phys. **22** (1961) 579; S. Weinberg, Phys. Rev. Lett. **1** (1967) 1264; A. Salam, Proc. 8th Nobel Symposium Stockholm 1968,ed. N. Svartholm (Almquist and Wiksell, Stockholm 1968) p.367; H. D. Politzer, Phys. Rep. **14** (1974) 129.
- [2] P. W. Higgs, Phys. Lett **12** (1964) 132, Phys. Rev. Lett. **13** (1964) 508; Phys. Rev. **145** (1966) 1156; F. Englert and R. Brout, Phys. Rev. Lett. **13** (1964) 321; G. S. Guralnik, C. R. Hagen and T. W. B. Kibble, Phys. Rev. Lett. **13** (1964) 585; T. W. B. Kibble, Phys. Rev. **155** (1967) 1554.

[3] N. Arkani-hamed, A. G. Cohen and H. Georgi, Phys. Lett. **B513**, (2001)232, [\[\protect\vrule width0pt\protect\href{http://arxiv.org/abs/hep-ph/0105239}{hep-ph/0105239}\]](http://arxiv.org/abs/hep-ph/0105239)

[4] N. Arkani-hamed, A. G. Cohen, T. Gregoire and J. G. Jacker, JHEP **0208**, (2002)020, [\[\protect\vrule width0pt\protect\href{http://arxiv.org/abs/hep-ph/0202089}{hep-ph/0202089}\]](http://arxiv.org/abs/hep-ph/0202089)

[5] N. Arkani-hamed, A. G. Cohen, E. Katz, A. E. Nelson, T. Gregoire and J. G. Wacker, JHEP **0208**(2002) 021, [\[\protect\vrule width0pt\protect\href{http://arxiv.org/abs/hep-ph/0206020}{hep-ph/0206020}\]](http://arxiv.org/abs/hep-ph/0206020)

[6] I. Low, W. Skiba and D. Smith, Phys. Rev. **D66**, (2002)072001, [\[\protect\vrule width0pt\protect\href{http://arxiv.org/abs/hep-ph/0207243}{hep-ph/0207243}\]](http://arxiv.org/abs/hep-ph/0207243)

[7] N. Arkani-hamed, A. G. Cohen, E. Katz and A. E. Nelson, JHEP **0207**(2002)304, [\[\protect\vrule width0pt\protect\href{http://arxiv.org/abs/hep-ph/0206021}{hep-ph/0206021}\]](http://arxiv.org/abs/hep-ph/0206021)

[8] For a recent review, see *e.g.*, M. Schmaltz, Nucl. Phys. Proc. Suppl. **117** 40-49 (2003), [\[hep-ph/0210415\]](http://arxiv.org/abs/hep-ph/0210415).

[9] T. Gregoire and J. G. Wacker, JHEP **0208**, 019 (2002) [\[\protect\vrule width0pt\protect\href{http://arxiv.org/abs/hep-ph/0206023}{hep-ph/0206023}\]](http://arxiv.org/abs/hep-ph/0206023)

[10] S. Dawson, S. Dittmaier and M. Spira, Phys. Rev. **D58** 40-49 (1998) [\[\protect\vrule width0pt\protect\href{http://arxiv.org/abs/hep-ph/9805244}{hep-ph/9805244}\]](http://arxiv.org/abs/hep-ph/9805244)

[11] E. W. N. Glover and J. J. van der BIJ, Nucl. Phys. **B309** 282-294 (1988)

[12] A. Krause, T. Plehn, M. Spira, P.M. Zerwas, Nucl.Phys. **B519** (1998)85-100; T. Plehn, M. Spira, P.M. Zerwas, Nucl.Phys. **B479** (1996)46; Jiang Yi, Han Liang, Ma

Wen-Gan, Yu Zeng-Hui and Han Meng, J. Phys. **G23** (1997) 385-400; Erratum-ibid. J. Phys. **G23** (1997) 1151.

[13] A. A. Barrientos Bendezu and B. A. Kniehl, Phys. Rev. **D64** (2001) 035006, [\[\protect\vrule{width0pt}{\protect\href{http://arxiv.org/abs/hep-ph/0103018}{hep-ph/0103018}}\]](http://arxiv.org/abs/hep-ph/0103018)

[14] U. Baur, T. Plehn and D. Tainwater, Phys. Rev. Lett. **89** (2002) 151801, [\[\protect\vrule{width0pt}{\protect\href{http://arxiv.org/abs/hep-ph/0206024}{hep-ph/0206024}}\]](http://arxiv.org/abs/hep-ph/0206024)

[15] C. Dib, R. Rosenfeld and A. Zerwekh, 'Higgs Production and Decay in the little Higgs Model', [\[\protect\vrule{width0pt}{\protect\href{http://arxiv.org/abs/hep-ph/0302068}{hep-ph/0302068}}\]](http://arxiv.org/abs/hep-ph/0302068)

[16] K.Hagiwara et al., Phys. Rev. D **66**,(2002)010001-29.

[17] M. Carena, D. Garcia, U. Nierste and C. E. M. Wagner, Nucl. Phys. **B577** (2000)88.

[18] T. Han, H. E. Logan, B.McElrath and L.T. Wang, Phy. Rev. **D67**,095004 (2003) [\[\protect\vrule{width0pt}{\protect\href{http://arxiv.org/abs/hep-ph/0301040}{hep-ph/0301040}}\]](http://arxiv.org/abs/hep-ph/0301040)

[19] T. Han, H. E. Logan, B.McElrath and L. T. Wang , Phys. Lett. **B563** (2003)191-202, [\[\protect\vrule{width0pt}{\protect\href{http://arxiv.org/abs/hep-ph/0302188}{hep-ph/0302188}}\]](http://arxiv.org/abs/hep-ph/0302188)

[20] C. Csaki, J. Hubisz, G. D. Kribs and P. Meade, Phys. Rev. **D67** (2003)115002, [\[\protect\vrule{width0pt}{\protect\href{http://arxiv.org/abs/hep-ph/0211124}{hep-ph/0211124}}\]](http://arxiv.org/abs/hep-ph/0211124)
Phys. Rev. **D68** (2003)035009, [\[\protect\vrule{width0pt}{\protect\href{http://arxiv.org/abs/hep-ph/9903282}{hep-ph/9903282}}\]](http://arxiv.org/abs/hep-ph/9903282)

[21] H. L. Lai,J. Huston, and S. Kuhlmann, Eur. Phys. J. C **12** (2000)375, [\[\protect\vrule{width0pt}{\protect\href{http://arxiv.org/abs/hep-ph/9903282}{hep-ph/9903282}}\]](http://arxiv.org/abs/hep-ph/9903282)

[22] F. Maltoni, Z. Sullivan, S. Willenbrock, Phys. Rev. **D67**, (2003)093005.

[23] J. L. Hewett, F. J. Petriello and T. G. Rizzo, JHEP **0310**(2003) 062, erb”[hep-ph/0211218]”.

Figure Captions

Fig.1 The one-loop Feynman diagrams of the subprocess $gg \rightarrow H^0 H^0$ in the LH model: (1)-(4) s-channel diagrams. (2)- (3), (5)-(6) box diagrams. (7) quartic diagrams. The notations u and d represent up-type and down-type quarks, respectively. The diagrams created by exchanging two external gluon lines and final Higgs boson lines are not shown.

Fig.2 The lowest order Feynman diagrams of the subprocess $b\bar{b} \rightarrow H^0 H^0$ in the LH model.

Fig.3(a) The relative effect of the LH on the cross section ($\delta = (\hat{\sigma}_{LH} - \hat{\sigma}_{SM})/\hat{\sigma}_{SM}$) for subprocess $gg \rightarrow H^0 H^0$ as the functions of $\sqrt{\hat{s}}$. Fig.3(a)-(1) is for $x = 0$ and Fig.3(a)-(2) for $x = 1/\sqrt{2}$ on the conditions of $f = 3.5$ TeV, $m_{H^0} = 150$ GeV. The full-line, dashed-line and dotted-line correspond to $\lambda_1/\lambda_2 = 1/2$, $\lambda_1/\lambda_2 = 1$ and $\lambda_1/\lambda_2 = 2$, respectively.

Fig.3(b) The cross sections of $gg \rightarrow H^0 H^0$ subprocess in the SM, the LH model and their difference $\hat{\sigma}_{LH} - \hat{\sigma}_{SM}$ as the functions of $\sqrt{\hat{s}}$ with $x = 0$, $f = 3.5$ TeV, $m_{H^0} = 150$ GeV and $\lambda_1/\lambda_2 = 1$.

Fig.4(a) The dependence of the ratio $\hat{\sigma}_{LH}/\hat{\sigma}_{SM}$ for the subprocess $gg \rightarrow H^0 H^0$ on the parameter x with $m_{H^0} = 150$ GeV and $\sqrt{\hat{s}} = 800$ GeV. The full-line, dashed-line and dotted-line -correspond to $\lambda_1/\lambda_2 = 1/2$, $\lambda_1/\lambda_2 = 1$ and $\lambda_1/\lambda_2 = 2$, respectively.

Fig.4(b) The total cross section and contributions of the box diagrams (including quartic diagrams), the triangle diagrams, interference between the box and triangle diagrams ($\hat{\sigma}_{LH} = \hat{\sigma}_{box} + \hat{\sigma}_{tri} + \hat{\sigma}_{int}$) for the subprocess $gg \rightarrow H^0 H^0$, as the functions of x with the conditions of $\sqrt{\hat{s}} = 800$ GeV, $m_{H^0} = 150$ GeV, $f = 3.5$ TeV and $\lambda_1/\lambda_2 = 1$. the full-line, dotted-line, dash-dotted line and dashed-line correspond to box diagrams, triangle diagrams, interference contributions and total cross section respectively.

Fig.4(c) The absolute value of original Higgs potential parameters λ_{ϕ^2} , $\lambda_{h\phi h}$, λ_{h^4} and $\lambda_{h\phi\phi h}$ as the functions of x with the conditions of $m_{H^0} = 150$ GeV and $f = 3.5$ TeV. The absolute value of coupling $g_{H^0 H^0 H^0}$ corresponding to the x value, is scaled on the upper axis.

Fig.5 The ratio of the total cross sections in the LH model and SM σ_{LH}/σ_{SM} for the process $pp \rightarrow H^0 H^0$ at the LHC, as the functions of $x (= 4fv'/v^2)$, with $f = 3.5$ TeV and $\lambda_1/\lambda_2 = 2$.

Fig.6 The ratio of the total cross sections σ_{LH}/σ_{SM} for the process $pp \rightarrow H^0 H^0$ at the LHC, as the functions of the Higgs boson mass m_{H^0} with the conditions of $f = 3.5$ TeV and $\lambda_1/\lambda_2 = 2$ in the LH model.

Fig.7 The total cross sections σ_{SM} and σ_{LH} for the process $pp \rightarrow H^0 H^0$ at the LHC, as the functions of the Higgs boson mass m_{H^0} with $f = 3.5$ TeV, $x = 0.9$ and $\lambda_1/\lambda_2 = 2$.

Fig.8 The total cross section σ_{LH} as the functions of the mass of the new heavy vector-like quark m_T with $m_{H^0} = 150$ GeV and $x = 1/\sqrt{2}$ in the LH model at the LHC.

ss

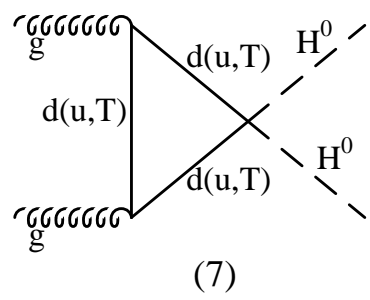
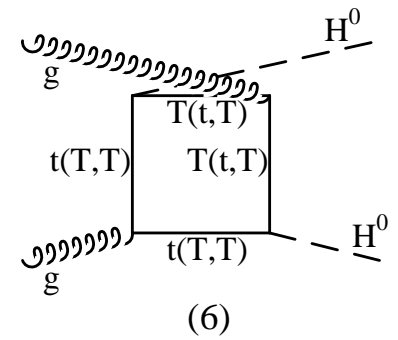
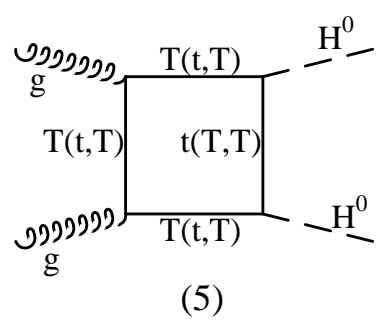
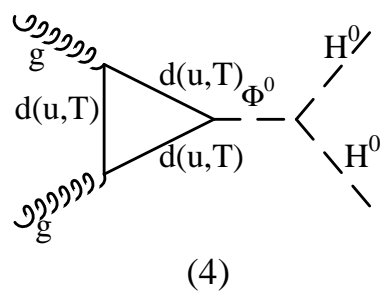
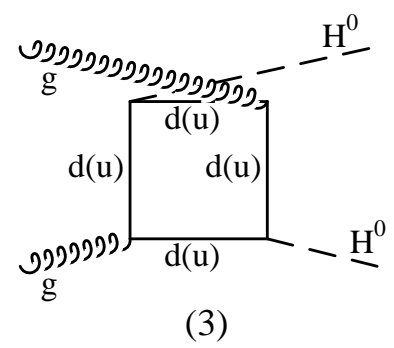
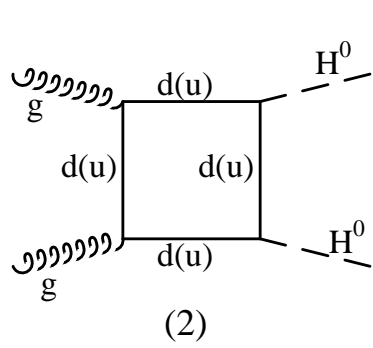
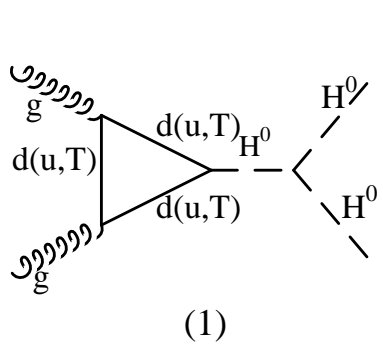


Fig.1

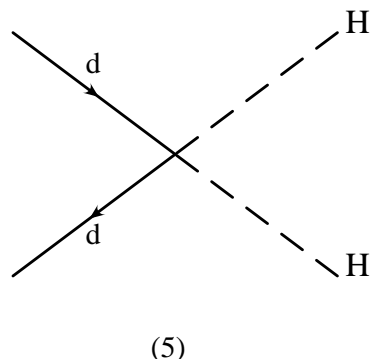
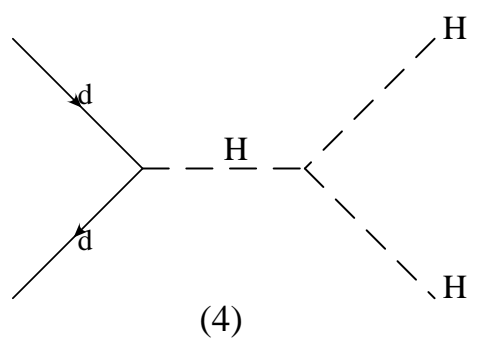
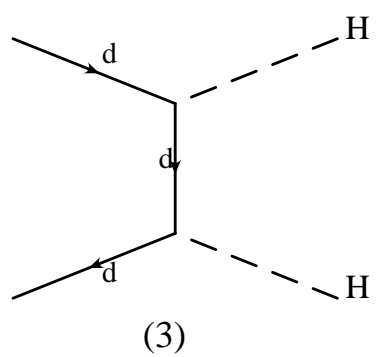
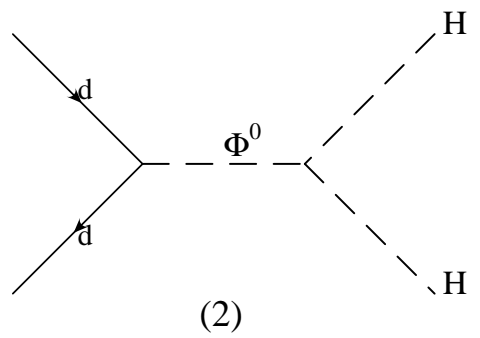
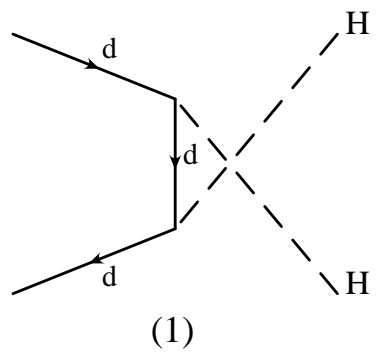


Fig.2

Fig .3(a)

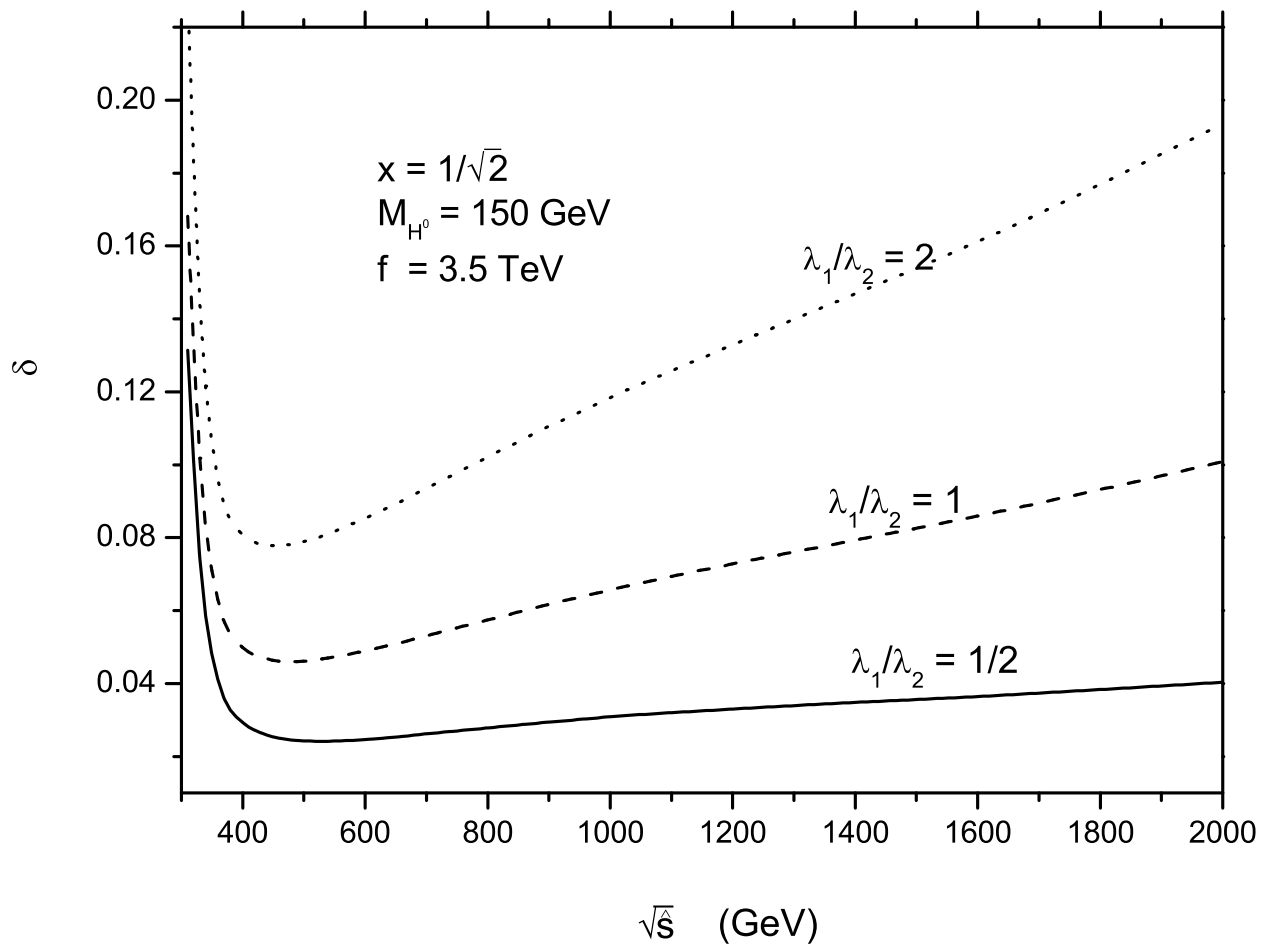


Fig . 3(b)

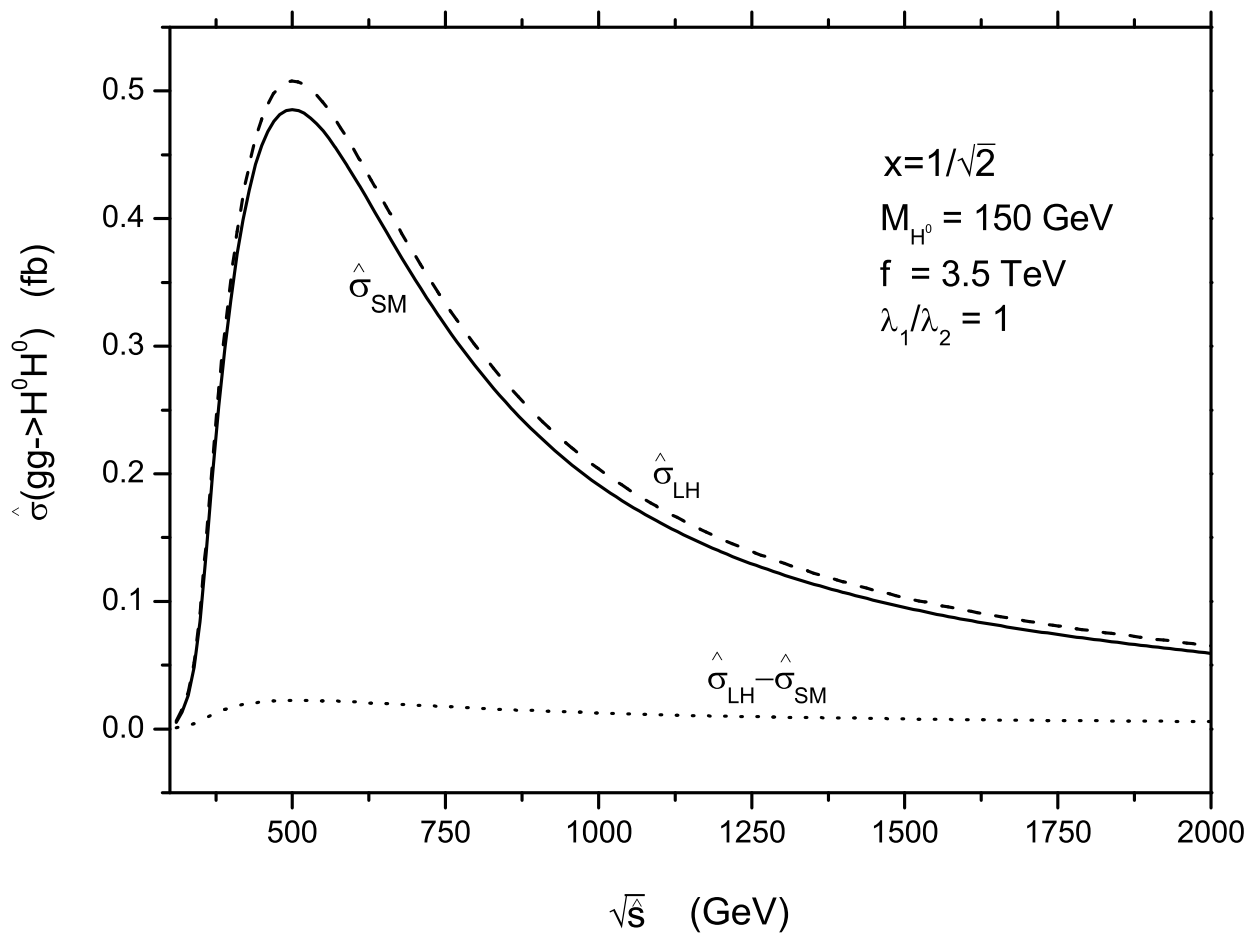


Fig . 4(a)

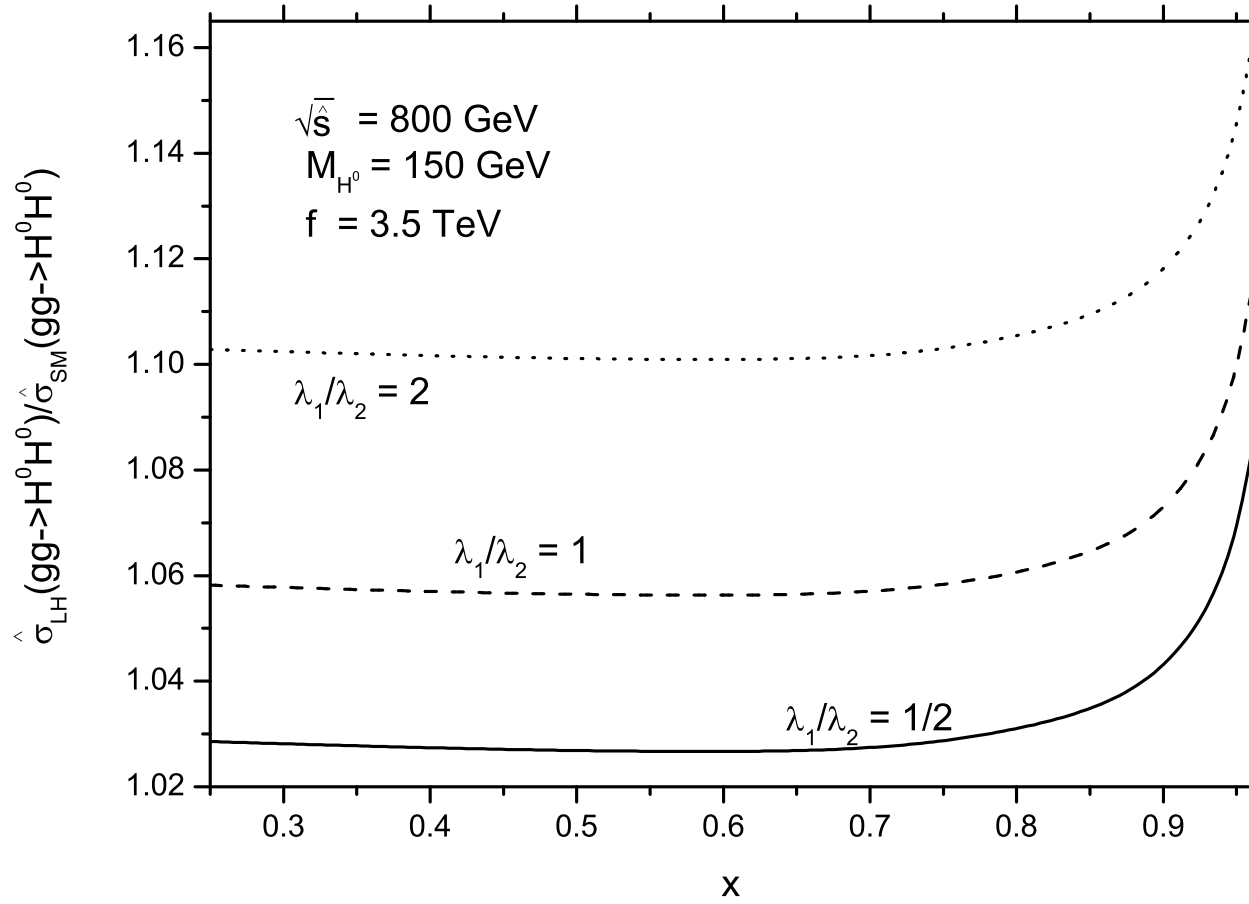


Fig . 4(b)

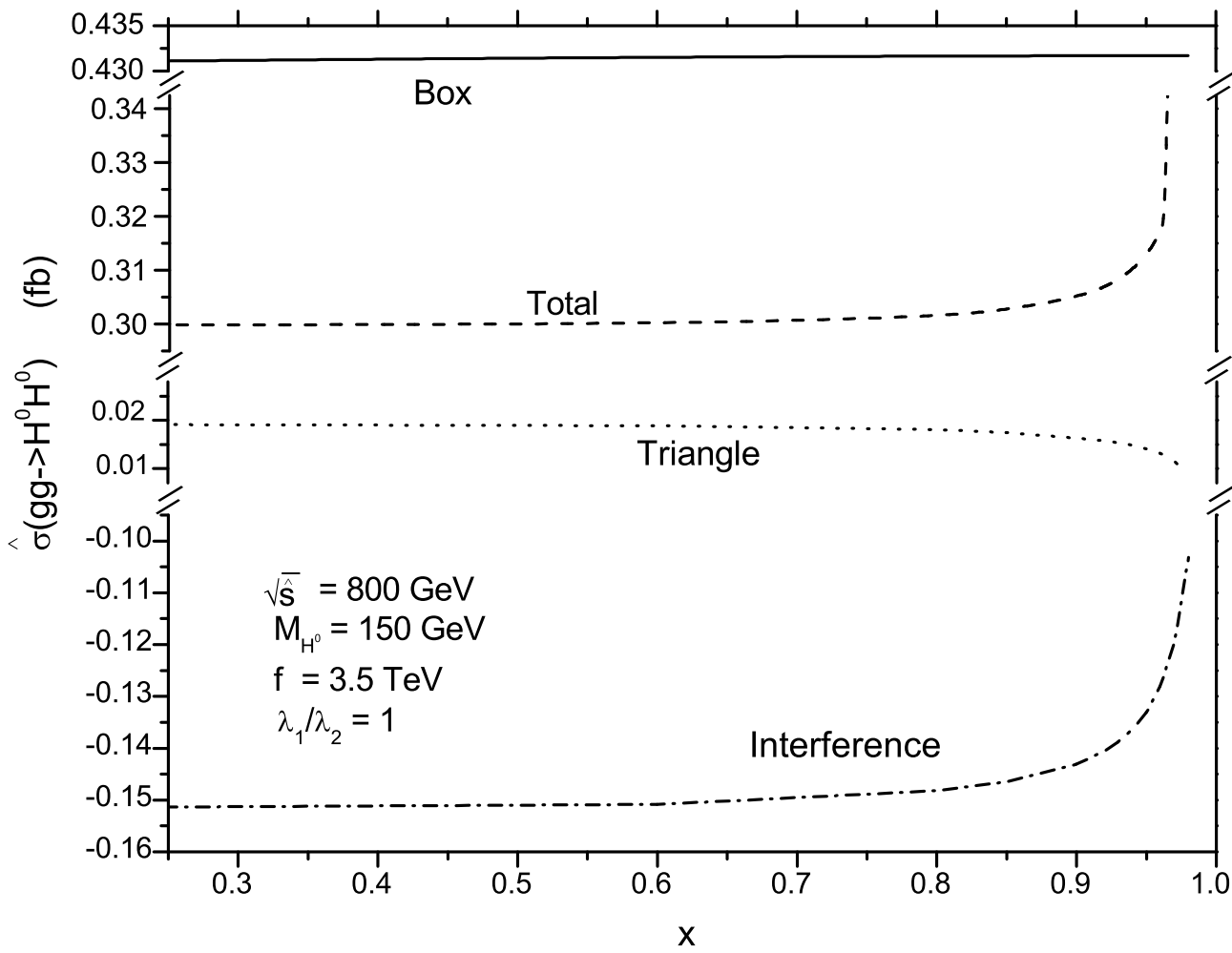


Fig. 4(c)

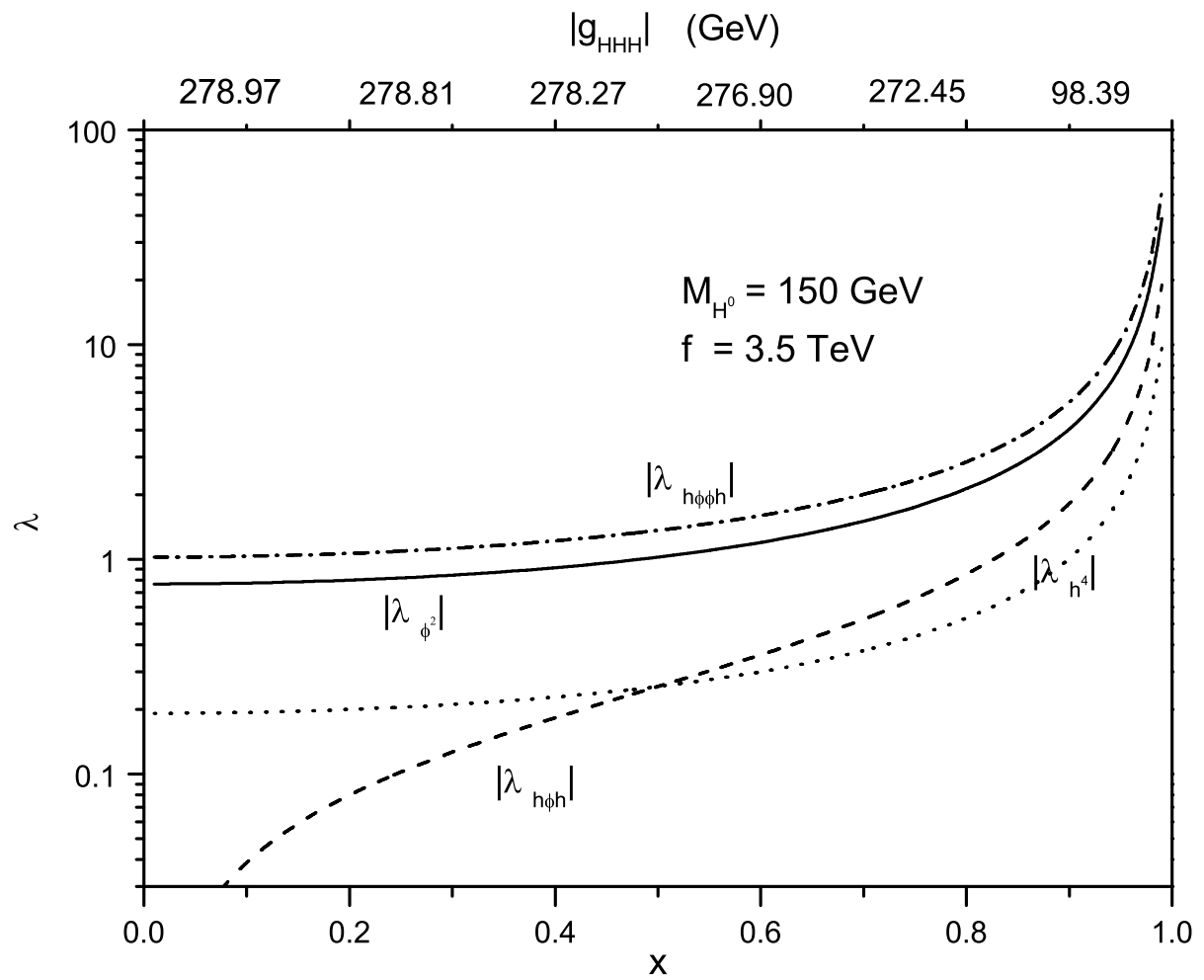


Fig . 5

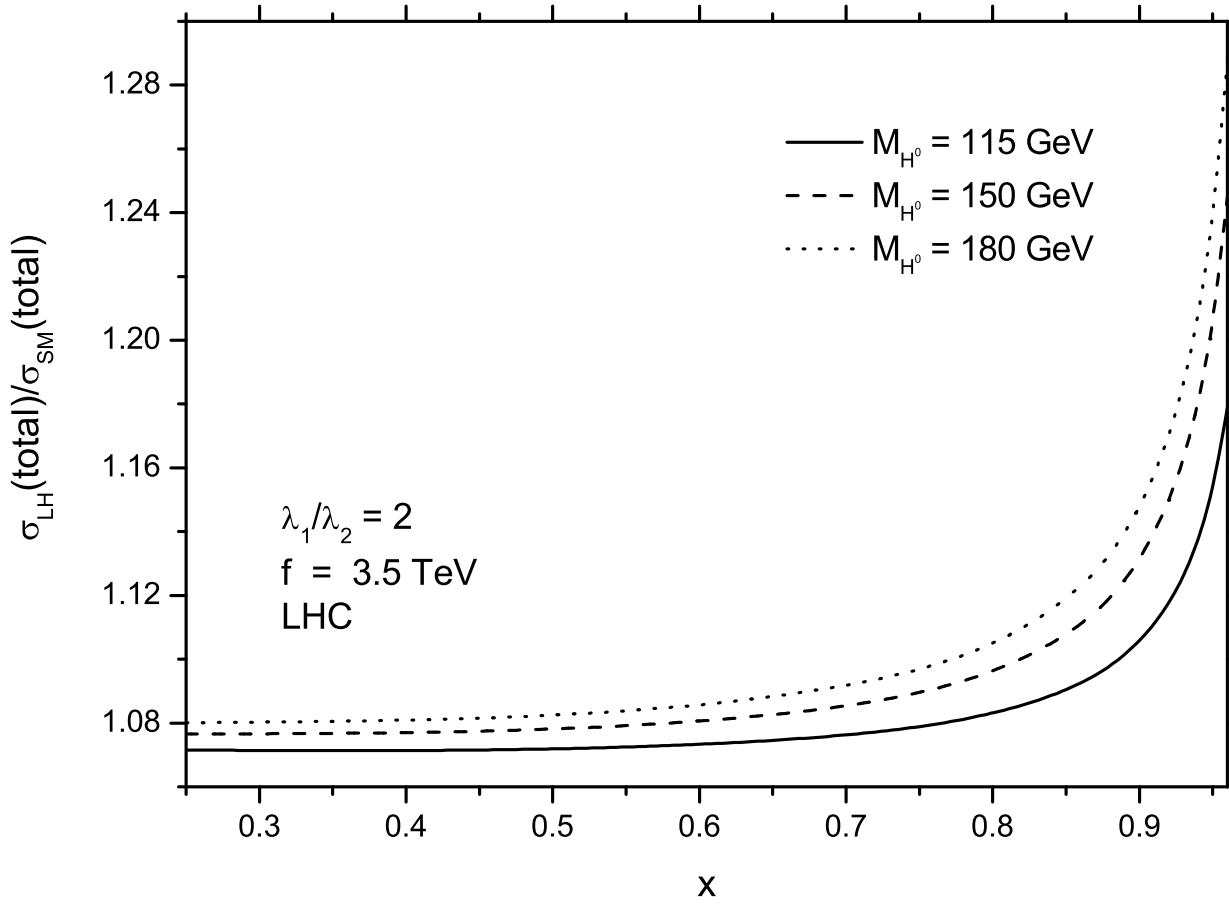


Fig . 6

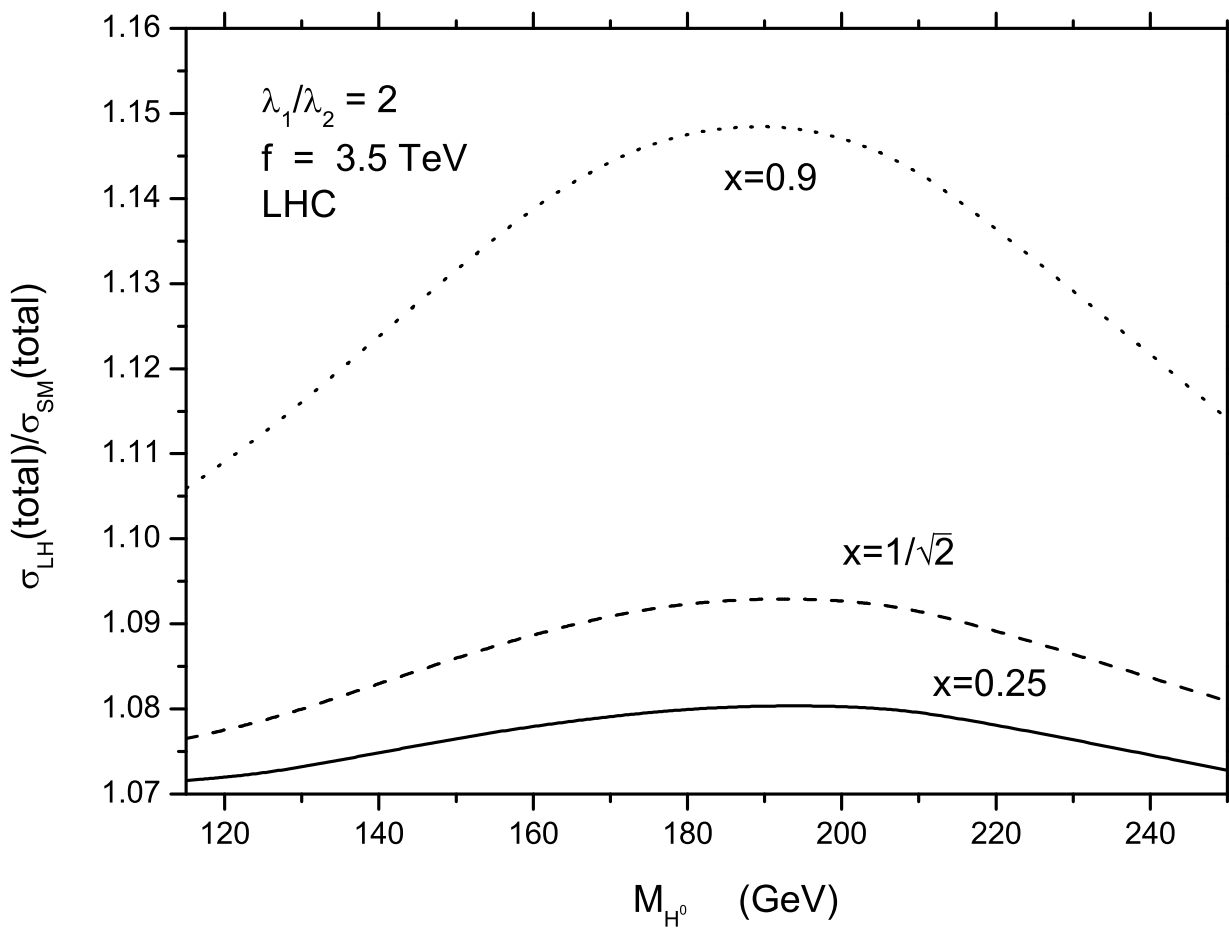


Fig . 7

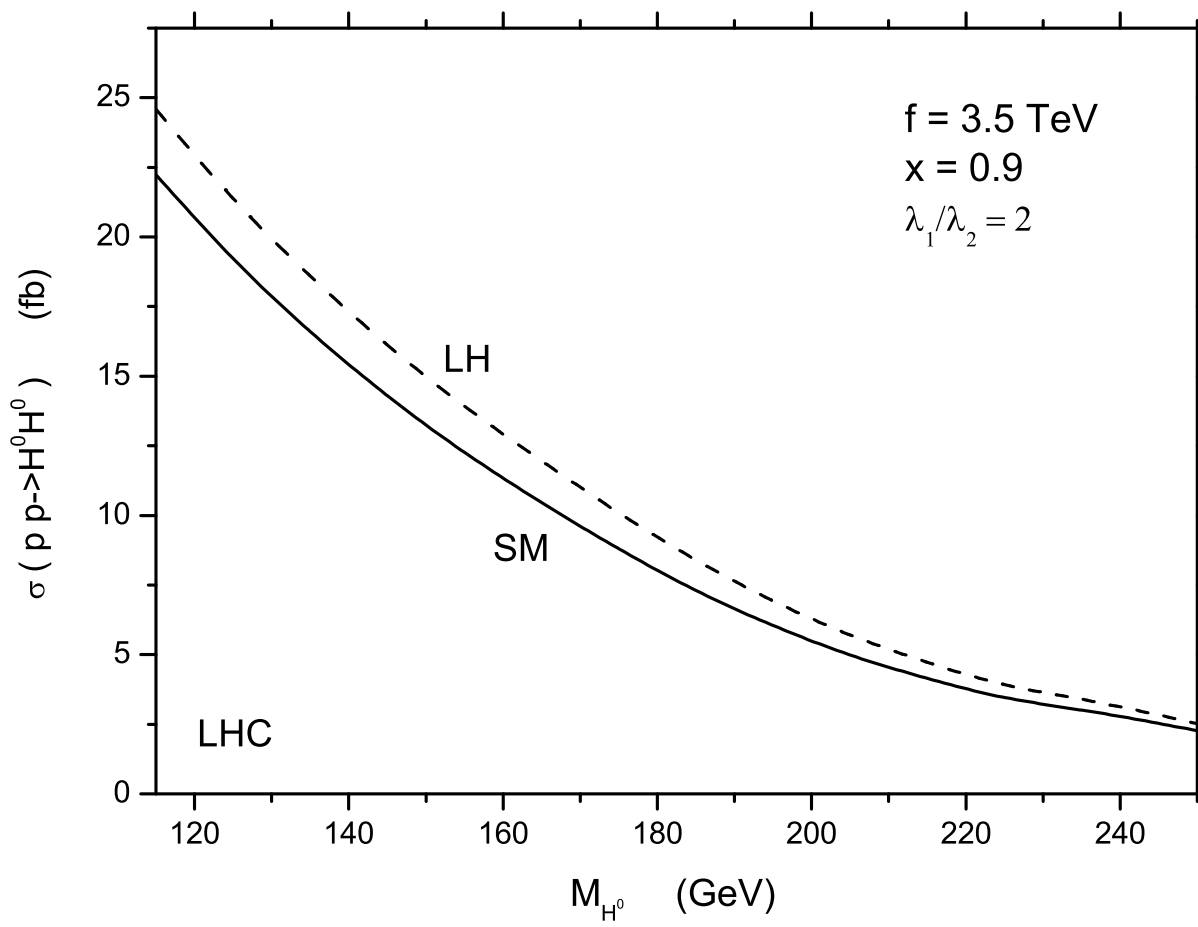


Fig . 8

